



INSTITUT DE FRANCE  
Académie des sciences

# *Comptes Rendus*

---

## *Géoscience*

### *Sciences de la Planète*

Daniele Maestrelli, Giacomo Corti, Marco Bonini, Domenico Montanari and Federico Sani

**Caldera collapse and tectonics along the Main Ethiopian Rift: reviewing possible relationships**


Volume 353, issue S2 (2021), p. 91-109

<<https://doi.org/10.5802/crgeos.63>>

**Part of the Special Issue:** Perspectives on alkaline magmas

**Guest editor:** Bruno Scaillet (Institut des Sciences de la Terre d'Orléans, CNRS, France)

© Académie des sciences, Paris and the authors, 2021.  
*Some rights reserved.*

 This article is licensed under the  
CREATIVE COMMONS ATTRIBUTION 4.0 INTERNATIONAL LICENSE.  
<http://creativecommons.org/licenses/by/4.0/>



*Les Comptes Rendus. Géoscience — Sciences de la Planète sont membres du  
Centre Mersenne pour l'édition scientifique ouverte  
[www.centre-mersenne.org](http://www.centre-mersenne.org)*



---

Perspectives on alkaline magmas / *Perspectives sur les magmas alcalins*

# Caldera collapse and tectonics along the Main Ethiopian Rift: reviewing possible relationships

Daniele Maestrelli<sup>\*, a</sup>, Giacomo Corti<sup>a</sup>, Marco Bonini<sup>a</sup>, Domenico Montanari<sup>a</sup>  
and Federico Sani<sup>b, a</sup>

<sup>a</sup> CNR-IGG, Consiglio Nazionale delle Ricerche, Istituto di Geoscienze e Georisorse,  
Via G. La Pira, 4, Firenze, Italy

<sup>b</sup> Dipartimento di Scienze della Terra, Università di Firenze, Via G. La Pira, 4, Firenze,  
Italy

*E-mails:* daniele.maestrelli@gmail.com, daniele.maestrelli@igg.cnr.it (D. Maestrelli),  
Giacomo.Corti@igg.cnr.it (G. Corti), marco.bonini27@gmail.com (M. Bonini),  
domenico.montanari@igg.cnr.it (D. Montanari), federico.sani@unifi.it (F. Sani)

**Abstract.** The Main Ethiopian Rift (MER) represents an area where volcanism and tectonics interact to create closely linked volcano-tectonic features. This linkage is paramount in the axial portion of the rift, where magmatic segments localize several large peralkaline eruptive centres. Many of them evolved into caldera collapse (the best preserved of which are younger than <1 Ma) generating large ignimbrites and registering the interaction between magmatism and tectonics along the MER. In this work we review the structure of the main collapsed calderas along the axial portion of the MER, to summarize the relationships between volcanism and tectonics proposed in the literature explaining their structural evolution. By doing this, we infer that tectonics had a strong influence in controlling the elongation of the majority of examined calderas. This control was induced by reactivation of inherited crustal fabrics or by stretching of the magma reservoirs under the MER regional stress field.

**Keywords.** Caldera collapse, Peralkaline calderas, Inherited faults, Regional tectonics, Caldera elongation, Tectonic controls, Main Ethiopian Rift.

Available online 5th July 2021

## 1. Introduction

The collapse of calderas is a volcano-tectonic process associated with the eruption/depletion or the lateral migration of magma from a magmatic chamber [e.g., Williams, 1941, Roche and Druitt, 2001, Druitt and Sparks, 1984, Lipman, 1997, Gudmundsson et al., 2016, Neal et al., 2019, Sigmundsson, 2019], causing

the volume of rock overlaying the latter to subside and form circular to elliptical depressions that may span from hundreds of meters to tens of kilometres in diameter. This process implies the eruption up to thousands of km<sup>3</sup> of magma, leading to a subsidence of the topographic caldera floor up to few kilometres [e.g., Druitt and Sparks, 1984, Lipman, 1984, 1997]. Caldera collapse is widely distributed in all the tectonic contexts [e.g., Geyer and Marti, 2008] and is a paramount process in continental rift settings, where extension and thinning of the lithosphere is associ-

---

\* Corresponding author.

ated with the inlet and emplacement of magma bodies at crustal levels. The Main Ethiopian Rift (MER), in the East African Rift System, does not make exception, showing hundreds of major volcanic centres along its whole length (and surrounding areas). Some of these volcanic systems eventually evolved into caldera collapse, leading to the emplacement of large ignimbritic sheets and plinian pumice fallout deposits with a peralkaline composition that cover the rift floor and a large part of the surrounding areas [Peccerillo *et al.*, 2003 and reference therein]. Indeed, magmatism and tectonics in the MER are crucially linked and their mutual relationships have been investigated since long time [e.g., Corti, 2009 and references therein]. Nonetheless, the active and passive role of magma ascent on tectonic processes is still widely debated [e.g., Bonini *et al.*, 1997, 2001, Boccaletti *et al.*, 1999, Ebinger and Casey, 2001, Kendall *et al.*, 2005, Casey *et al.*, 2006, Corti, 2008, Bastow *et al.*, 2010, Wadge *et al.*, 2016], and similarly is the role of pre-existing and rift-related tectonic structures during caldera collapse [e.g., Acocella *et al.*, 2002, Rampey *et al.*, 2010]. Calderas in the MER have focused the interest of researchers since the early stages of geological exploration of the rift, and many studies contributed to document their volcanic, petrological and structural evolution [e.g., Di Paola, 1971, 1972, Mohr and Wood, 1976, Mohr *et al.*, 1980, Spera and Crisp, 1981, WoldeGabriel *et al.*, 1992, Le Turdu *et al.*, 1999, Acocella *et al.*, 2002, Peccerillo *et al.*, 2003, Casey *et al.*, 2006, Rampey *et al.*, 2010, Giordano *et al.*, 2014, Hutchison *et al.*, 2016a,b, Corti *et al.*, 2018, Lloyd *et al.*, 2018]. Despite caldera collapse is generally accommodated by a system of outward-dipping reverse faults and inward-dipping normal ring faults [e.g., Acocella, 2007], existing tectonic structures may interact with caldera-related structures, and influence the eccentricity of the caldera system. Several researches claimed, in fact, an important role of tectonic structures on the evolution of such systems, indicating that both inherited (older) and rift-related structures are key factors controlling the collapse [e.g., Acocella *et al.*, 2002, 2004, Holohan *et al.*, 2005, 2008, Maestrelli *et al.*, 2020, 2021a,b, Bonini *et al.*, 2021].

In this work, we aim to review the structural characteristics of the main collapsed calderas occurring along the magmatic segments of the MER, to discuss their setting in the frame of the tectonic evolution of

the area. We finally aim to summarise in which cases tectonic structures may have influenced the development of the examined caldera collapse systems.

## 2. MER tectono-magmatic evolution

The MER represents the northernmost, ~1000 km-long, sector of the East African Rift System (EARS), and results from relative motion between the Nubia and Somalia plates, which is occurring in a roughly E–W direction at rates of ~4–6 mm/yr [e.g., Billham *et al.*, 1999, Saria *et al.*, 2014]. The MER is classically subdivided in three main sectors reflecting different stages of evolution [e.g., Hayward and Ebinger, 1996, Agostini *et al.*, 2011a]. The Northern MER (N-MER; Figure 1), extending from the Afar Depression to the Lake Koka area, is the most evolved sector, and is marked by magma-dominated processes. The Southern MER (S-MER) has its northern boundary in the Lake Awasa area, and is nowadays experiencing fault-dominated extensional processes, with limited volcanism, reflecting the youngest stage of evolution. The Central MER (C-MER), located halfway through the MER, shows intermediate features. Such different maturity stages, varying from N to S along the MER, may suggest that this rift is propagating southward toward the Turkana Depression, where it links with the Kenya Rift [e.g., Corti *et al.*, 2019], although the timing of rift initiation and propagation is complex and still not fully understood [Balestrieri *et al.*, 2016].

The MER is marked by large boundary faults, formed asynchronously along the rift and characterized by a vertical offset >1 km [e.g., Boccaletti *et al.*, 1998]; these fault systems show different orientation in the N-MER, C-MER, and S-MER sectors, ranging from ~N40° E in N-MER to N30° E in the C-MER and varying between N0° E to N20° E in S-MER (Figure 1). Geological and geophysical data indicate that the large boundary faults have been active between 11 and 2 Ma in the N-MER, whereas they are still active in the C-MER and S-MER. The floor of the present-day rift valley is characterized by a pervasive pattern of short, right-stepping en-echelon faults with throws <100 m and trending obliquely to the rift boundaries. Similarly to the boundary faults, these axial structures, classically named Wonji Fault Belt [WFB; Mohr, 1962b, 1967; Meyer *et al.*, 1975], show different characteristics in the three MER sectors: they are oriented ~N20° E in the N-MER, ~N12° E in

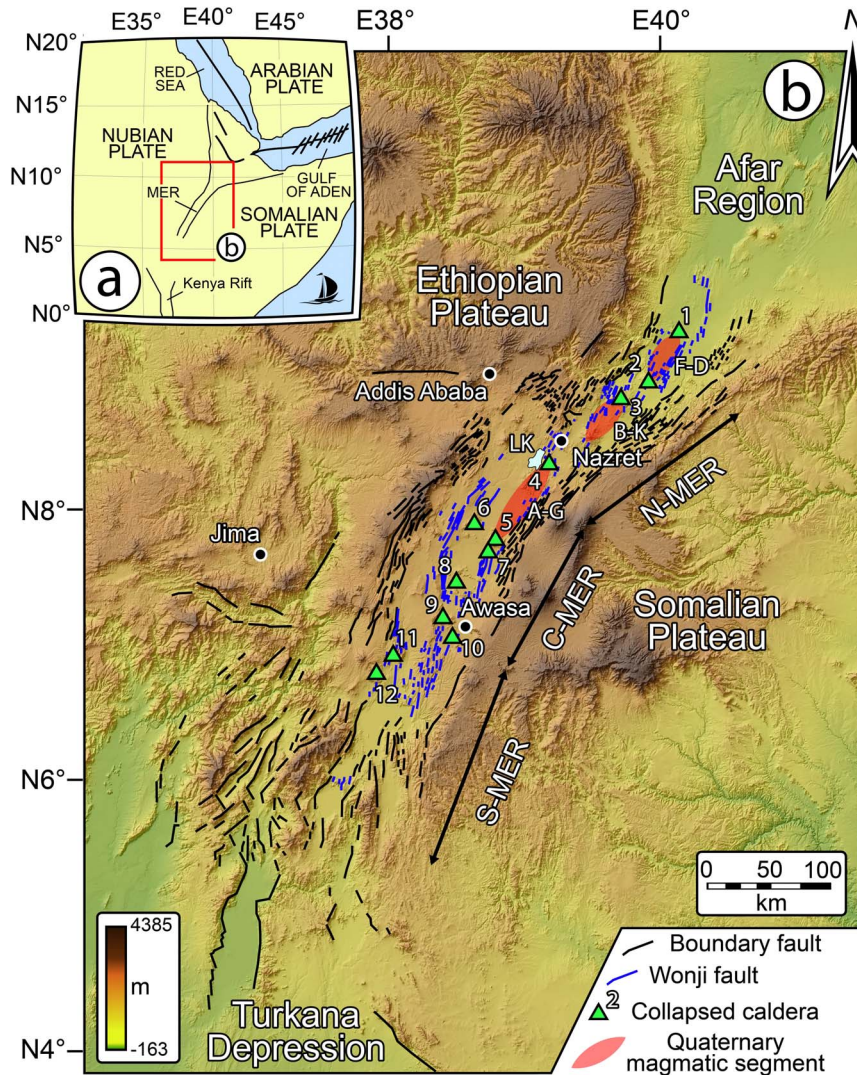


**Figure 1.** The Main Ethiopian Rift. Black lines mark the major boundary faults, while blue lines show the Wonji faults. Green triangles indicate the calderas described in this study. LK: Lake Koka. (1) Dofen Volcanic Complex (DVC); (2) Fantale; (3) Kone Volcanic Complex (KVC); (4) Gedemsa; (5) Aluto; (6) Gademotta; (7) Munesa; (8) Shala; (9) Corbetti; (10) Awasa; (11) Duguna; (12) Hobitcha. F–D: Fantale–Dofen magmatic segment; Boset–Kone magmatic segment; Aluto–Gedemsa magmatic segment.

the C-MER and roughly N–S in the S-MER; in the N-MER the WFB started forming at around 2 Ma, when the deformation shifted from the boundary faults to the axial portion of the rift, whereas they are in an incipient stage in the C-MER and almost absent in the S-MER [e.g., Agostini et al., 2011a]. Kinematics of WFB faults typically varies between pure dip-slip to slight oblique-slip displacement (dextral or sinis-

tral), consistent with a roughly E–W trending Late Quaternary extension direction (N90°–95°; Agostini et al., 2011b). In the N-MER, the WFB are closely associated with the Quaternary volcanic activity, with alignment of eruptive centres and volcano-tectonic features defining the so-called axial magmatic segments [e.g., Ebinger and Casey, 2001, Casey et al., 2006; Figure 1]. Active faults at the WFB cross-cut

several calderas and facilitate post-caldera basaltic and silicic eruptions forming scoria cones and lava flows [Fontijn *et al.*, 2018]. The axial segmentation of the volcano-tectonic activity is mimicked in a similar segmentation at depth. Tomographic analysis revealed indeed segmented low velocities zones, interpreted as the loci of enhanced melt production from the mantle, suggesting that magma generation and faulting at surface are intimately linked [Keranen *et al.*, 2004, Bastow *et al.*, 2005]. The development of the WFB in the N-MER has been interpreted as reflecting a change in the deformation style from ~2 Ma [e.g., Meyer *et al.*, 1975], with the deactivation of the large-throw boundary faults and migration of strain and volcanic activity to the centre of the rift depression [Morton *et al.*, 1979]. As outlined above, transition from axial tectono-magmatic activity and magma-dominated deformation in the N-MER to marginal faulting with limited volcanism in the S-MER has been interpreted to reflect a North to South transition from more advanced to less advanced rifting stages.

Extension in the Ethiopian region was predated by a complex pre-Tertiary tectonic history responsible of several heterogeneities that influenced rift localization and evolution at both regional scale and local scale [e.g., Mohr, 1962b, Keranen and Klemperer, 2008, Bastow *et al.*, 2008, Keranen *et al.*, 2009]. This phase was followed by an intense basaltic volcanic activity (since ~45 Ma) emplacing the so-called Trap series, characterised by tholeiitic to alkaline lava flows [e.g., Kieffer *et al.*, 2004, Rooney, 2017] intercalated with silicic volcanics to form an up to 3000 m volcanic pile [e.g., Mohr and Zanettin, 1988]. This activity continued during the Miocene with the building of large volcanic edifices on the plateaus surrounding the rift [e.g., Kieffer *et al.*, 2004], and with a second phase of widespread basaltic activity between 12 and 8 Ma [e.g., Bonini *et al.*, 2005]. Later on, at ~6–8 Ma, a major pulse in volcanic activity was confined within the developing rift valley; this activity was characterized by the alternate eruption of large ignimbrite deposits and basaltic magmatism [Boccaletti *et al.*, 1999, Trua *et al.*, 1999]. During the Quaternary, this typical bimodal magmatic activity, mainly occurring as pulsed phases, localized in the axial magmatic segments of the N-MER [e.g., Casey *et al.*, 2006, Hutchison *et al.*, 2016a] synchronously to WFB development, generating tra-

chyte and rhyolite pyroclastites from central emission points (strato-cones and caldera complexes) and subordinated basalts from fissural eruptions [e.g., Chernet and Hart, 1999, Boccaletti *et al.*, 1999, WoldeGabriel *et al.*, 1999, Casey *et al.*, 2006].

The history of the MER, since pre-Tertiary times, therefore shows how tectonics and volcanism are interrelated, indicating that inherited structures at places influenced volcanic activity by localizing eruptions, aligning volcanic centres and guiding dyke orientation [e.g., Wadge *et al.*, 2016]. It was proposed that large silicic centres were emplaced at the tip of magmatic segments, where reduced stress favoured long residence time and consequent magma evolution [e.g., Le Turdu *et al.*, 1999, Peccerillo *et al.*, 2003; Figure 1]. Alternatively, other works suggest that deformation at the centre of the segments is mainly controlled by magmatism, while it is predominantly brittle at the segment tips [e.g., Kurz *et al.*, 2007]. Several volcanoes along the MER evolved as caldera collapse structures, and many authors suggested a role of inherited faults on the development of certain caldera features [e.g., Acocella *et al.*, 2002]. Besides, other studies suggest that tectonic activity was subordinated to magmatism, and that collapsed calderas were not controlled by inherited fabrics [e.g., Casey *et al.*, 2006]. In the following paragraphs, we review the main (twelve) caldera collapses (Figure 1), highlighting their structural setting and aiming to disclose whether tectonic processes played a role during their evolution.

### 3. Collapsed calderas along the MER

We describe collapsed calderas and their structural setting from N to S, grouping them according to the three main rift sectors (N-MER, Figure 2; C-MER, Figure 3; S-MER, Figure 4). This choice reflects the difference in the evolutionary stage of the three sectors, consequently influencing the setting in which caldera collapse occurred. Characteristics of Ethiopian calderas have been reported in Table 1, which has been compiled from the literature and new data deriving from this study.

**Table 1.** Summary of caldera features described in this work and compiled from literature

Name	MER sector	Lat.	Long.	Age oldest	Age youngest	Axial ratio ( $L_A/S_A$ ) <sup>(3)</sup>	Long axis trend	Rocks	Caldera features	Area	Strain $\ln(L_A/S_A)$ <sup>(3)</sup>
Dofen	N	9.35°	40.13°	1.7 Ma <sup>(1)</sup>	Historic	2.56 <sup>(3)</sup>	ed N113° E	Trachy-basaltic lava flows, rhyolite flows and domes <sup>(1)</sup>	Summit caldera on a strained magmatic edifice	1 × 1 km, considering the summit collapse	0.940 <sup>(3)</sup>
Fantale	N	8.98°	39.90°	168 ± 38 Ka <sup>(2)</sup>	1820 a.d. <sup>(3)</sup>	1.58 <sup>(2)</sup> 1.67 <sup>(3)</sup> 1.77 <sup>(3)</sup> 1.61 <sup>(3)</sup> 1.64 <sup>(3)</sup>	N112° E <sup>(2)</sup> N111–114° E <sup>(3)</sup> N107 ± 4° E <sup>(4)</sup>	Ignimbrite, pumices, ash fallout, obsidian, rhyolites, basaltic lavas <sup>(3)</sup>	Nested inside major caldera; Fault-controlled margins	2.9 × 4.4 km <sup>(2)</sup> 2.5 × 4.5 km <sup>(4)</sup>	0.457 0.513 <sup>(3)</sup> 0.571 <sup>(3)</sup> 0.476 <sup>(3)</sup>
Kone (3 main cald.: Kone or Gariboldi, Korke, Birenti)	N	8.84°	39.69°	<0.32 Ma <sup>(5)</sup>	1810 a.d. <sup>(5)</sup>	1.49 <sup>(3)</sup>	N94 ± 17E <sup>(4)</sup>	Pumices and ash fallout, ignimbrites and rhyolitic lavas, trachytes, basalt flows <sup>(3)</sup>	Nested; Fault-controlled margins	5.0 × 7.5 km <sup>(4)</sup> 95 km <sup>2(5)</sup>	0.399
Gedemsa	N	8.36°	39.17°	0.88 Ma <sup>(3)</sup> 0.8 Ma <sup>(4)</sup>	0.29–0.2 Ma <sup>(3)</sup> 0.32–0.26 Ma <sup>(6)</sup> 0.1 Ma <sup>(4)</sup>	1.315 <sup>(2)</sup> 1.23 <sup>(3)</sup>	N75° E <sup>(2)</sup> N86° E <sup>(4)</sup>	Trachytic, rhyolitic and obsidian lavas, Ignimbrite, surges and fallout <sup>(4,7)</sup>	Fault-controlled margins	7.3 × 9.6 <sup>(2)</sup> 7 × 9 km <sup>(4)</sup>	0.274 0.207 <sup>(3)</sup>
Aluto	C	7.74°	38.78°	0.27–0.15 Ma <sup>(8)</sup> 316–306 Ka <sup>(9)</sup>	21–9.4–2 Ka <sup>(8)</sup> >60 Ka <sup>(9)</sup>	1.72 <sup>(2)</sup>	N90° E <sup>(8)</sup>	Trachytic, Ignimbrites, pumices, obsidian <sup>(9)</sup>		8.6 × 5.0 km <sup>(9)</sup>	0.542
Shala (O'a)	C	7.47°	38.50°	0.24 Ma <sup>(8)</sup>	0.18 Ma <sup>(8)</sup>	1,143 (O'a)	N105–110° E	Ignimbrite, pumices, rhyolites, basalts <sup>(4,8)</sup>	Nested?	16 × 14 km (O'a)	0.133
Corbetti	C/S	7.20°	38.36°	0.24 Ma <sup>(8)</sup>	0.18–0.1 Ma <sup>(8,11)</sup>	1.43 <sup>(2)</sup>	N104° E <sup>(2)</sup> N135° E <sup>(7,10)</sup>	Ignimbrite, pumices <sup>(9)</sup>	Nested? Fault-controlled margins	12 × 10 km <sup>(7,10)</sup>	0.357
Awasa	C/S	7.04°	38.43°	1.0 Ma <sup>(12)</sup> 1.85–1.1 Ma <sup>(11)</sup>	~1900 a.d. <sup>(12)</sup>	1.75 1.333	≈E–W*	Ignimbrite	Nested?; Strongly eroded	35 × 20 30 × 40 km <sup>(12)</sup>	0.560 0.288
Duguna	S	6.91°	38.01°	0.46–0.43 Ma <sup>(14)</sup>	?	1,333	N35° E	Pumices, ash fall <sup>(13)</sup>		8 × 6 km	0.288
Hobitcha	S	6.79°	37.88°	?	?	?	N110° E	Rhyolites	Strongly eroded	~10 km diam.	?

Reference legend: (1) Chernet, 2005; (2) Hunt et al., 2019 and reference therein; (3) Casey et al., 2006; (4) Acocella et al., 2002 and reference therein; (5) Rampey et al., 2010 and reference therein; (6) Peccerillo et al., 2003; (7) Di Paola, 1971; (8) Le Turdu et al., 1999; (9) Hutchison et al., 2016b and reference therein; (10) Di Paola, 1972; (11) Hutchison et al., 2016a; (12) Newhall and Dzurisin, 1988; (13) Corti et al., 2013 and reference therein; (14) Bigazzi et al., 1993. Where not specified the data here reported belong to this study. ed.: edifice. The strain (or natural strain) is calculated, following Casey et al. [2006], as the natural logarithm of the caldera long axis ( $L_A$ ) and short axis ( $S_A$ ) ratio.

\* The elongation of Awasa is roughly E–W, but the presence of erosional embayments does not allow for a clear definition of the caldera major axis.

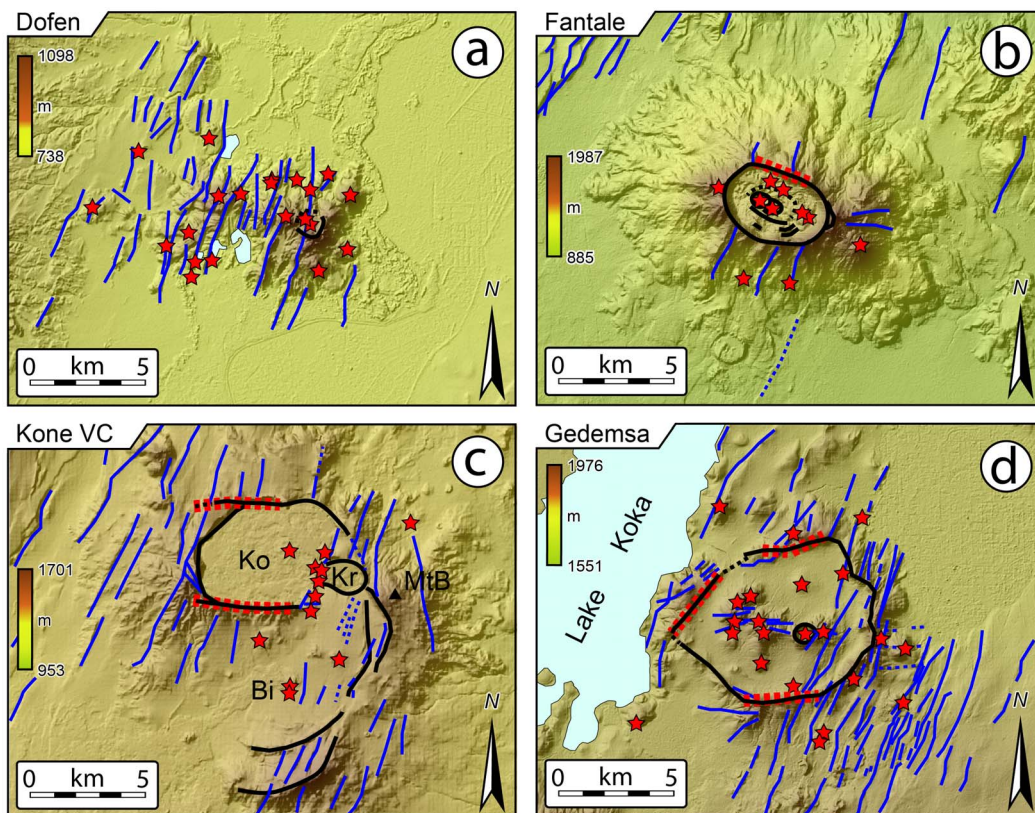


**Figure 2.** (a) Dofen Volcanic Complex. This volcanic complex, defining the northern tip of the Dofen–Fantale magmatic segments, shows a small collapsed caldera. Structures and emission points are mapped after Casey *et al.* [2006]. (b) Fantale Caldera showing NW–SE elongation. Caldera and tectonic structures are mapped after Acocella *et al.* [2002]. (c) Kone Volcanic Complex (KVC), which is composed of the remnants of the Birenti Caldera (Bi), Kone Caldera (Ko) and the Korke Embayment (Kr). MtB: Mount Birenti (black triangle). Caldera location is indicated in Figure 1. Caldera and tectonic structures are mapped after Acocella *et al.* [2002] and Rampey *et al.* [2010]. (d) Gedemsa Caldera showing two major rectilinear caldera walls. Caldera and tectonic structures are mapped after Korme *et al.* [1997], Acocella *et al.* [2002] and Hutchison *et al.* [2016a]. Newly mapped tectonic structures are interpreted on 30 m resolution ALOS DEMs. Black thick lines indicate caldera structures (dashed black lines for uncertain caldera structures), while blue lines indicate tectonic structures. Red stars indicate volcanic emission points. Thick red dashed lines indicate fault-controlled caldera margin, as inferred by Acocella *et al.* [2002] and Hunt *et al.* [2019].

### 3.1. *N-MER calderas*

#### 3.1.1. *Dofen volcanic complex (DVC)*

The felsic Dofen volcanic complex (DVC; Figures 1b and 2a) is located at the northern tip of the Dofen–Fantale magmatic segment and is represented by a NW–SE elongated relief (Figure 5). This relief has been interpreted to be a strained volcanic

edifice in a  $\sim$ N110° E direction [Casey *et al.*, 2006], nowadays dissected by several NNE–SSW trending faults and fractures (Figures 2a and 5). The volcanic system lays, together with the Fantale Caldera more to the south, within an east-dipping half-graben bounded by a 60–80 m-high fault scarp [Casey *et al.*, 2006]. K/Ar dating ascribes the Dofen complex to 1.7 Ma but historical lava flows testify ongoing activ-

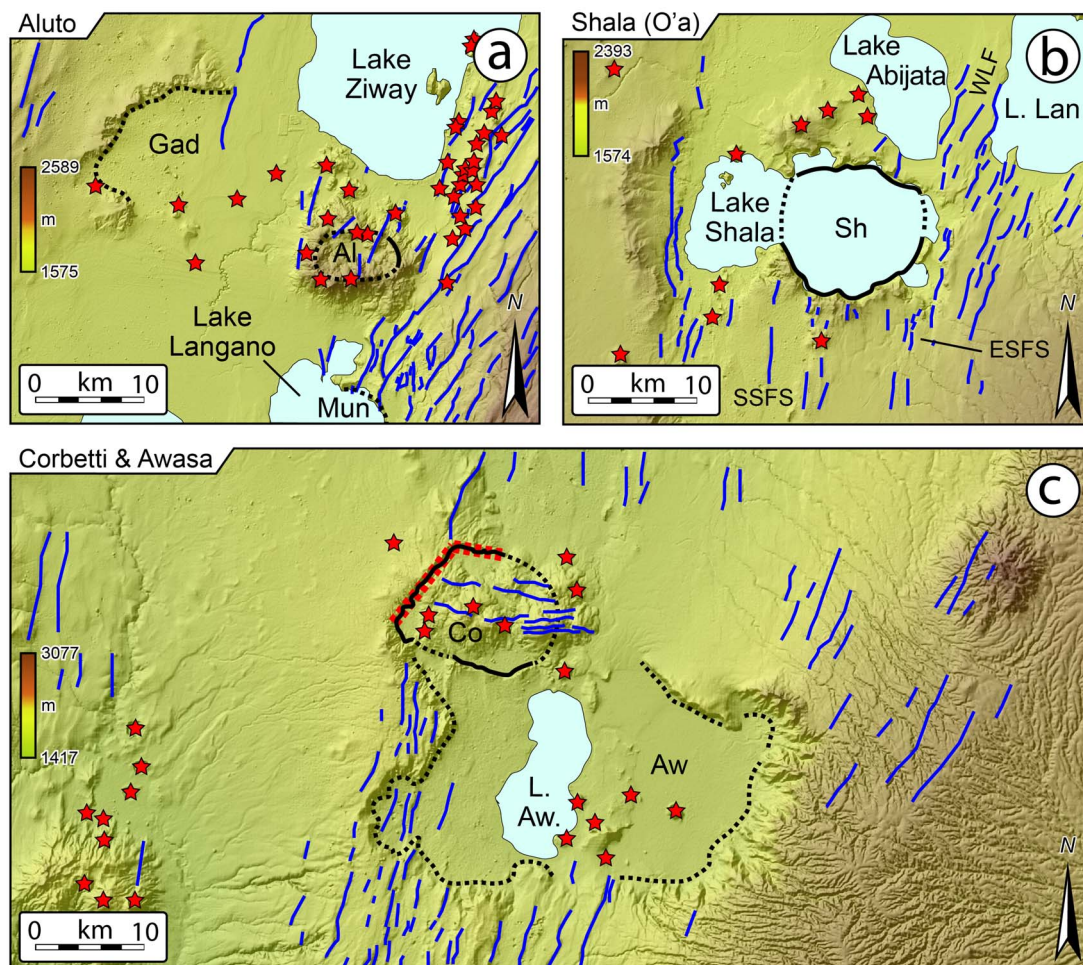


**Figure 3.** (a) Aluto Caldera (Al) and the remnants of the Gademotta (Gad) and Munesa (Mun) calderas. Structures are redrawn after Hutchison et al. [2016a,b]. L. Lan.: Lake Langano. (b) Shala Caldera. Structures are redrawn after Hutchison et al. [2016a,b]; Mohr et al. [1980] and Le Turdu et al. [1999]. L. Lan.: Lake Langano; SSFS: Southern Shala Fault System; ESFS: Eastern Shala Fault System; WLF: West Lango Fault. (c) Corbetti (Co) and Awasa (Aw) calderas. L. Aw.: Lake Awasa. Structures are redrawn and modified after Di Paola [1971], Korme et al. [1997], Hutchison et al. [2016a], Lloyd et al. [2018] and Hunt et al. [2019]. Caldera location is indicated in Figure 1. Symbol and legend are as in Figure 2.

ity [Chernet, 2005; Table 1]. In its central portion, normal faults with throw >100 m dismantled what Casey et al. [2006] refer to a “caldera complex”. Nonetheless, no clear evidence of large caldera structures can be interpreted from DEMs, except for the small depression (~1 km in diameter) occurring in the eastern portion of the volcanic complex. Several emission points align with NE–SW trending structures, interpreted by Casey et al. [2006] as the surface expression of dyke segments.

### 3.1.2. *Fantale caldera*

Fantale is one of the most active volcanoes in the MER and is located at the southern tip of the Dofen–Fantale magmatic segment [Figure 1; Casey et al., 2006]. Its volcanic history was dominated by eruption of intermediate and silicic volcanics, ranging from ignimbrite pumices and ash falls in the early stages to lava flows (obsidian and rhyolites) in later stages [Hunt et al., 2019]. Obsidian flows and basaltic



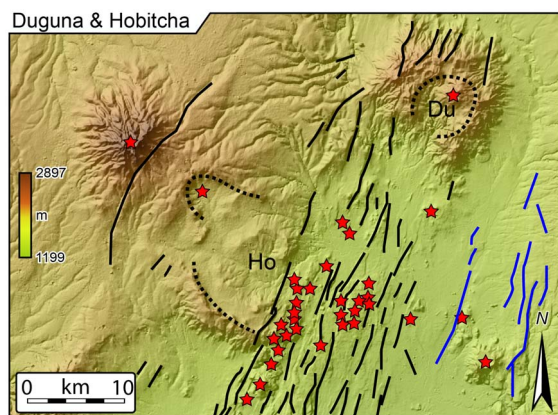


**Figure 4.** Duguna volcanic complex with summit caldera collapse and the remnants of the Hobitcha Caldera. Structures are redrawn after Corti *et al.* [2013], Chernet [2011] and Minissale *et al.* [2017]. Black lines indicate rift boundary faults, while blue lines indicate the axial Wonji Faults. All other symbols are as those in Figure 2. Caldera location is indicated in Figure 1.

lavas were erupted in 1820 [Gibson, 1969]. Acocella *et al.* [2002] identified in the area NNE–SSW trending WFB faults (mean trend  $N23^{\circ} E \pm 5^{\circ}$ ), with a maximum displacement of 100 m, and described the elliptical caldera ( $\sim 2.5 \times 4.5$  km, or  $2.9 \times 4.4$  km, following Hunt *et al.*, 2019; Table 1) as characterized by a topographic subsidence of 100 m (Figures 2b and 5; Table 1). Inside Fantale, a smaller nested caldera (40 m deep) is visible. WNW–ESE trending vertical faults crosscut the caldera rim and several monogenic vents are reported by Acocella *et al.* [2002] in the caldera depression as well as along the rim, organized in trails sub-parallel to caldera elongation. Outside the caldera, Acocella *et al.* [2002] report vent distribution as mainly controlled by NNE–SSW trending Wonji structures, with no evidence of WNW–ESE trending structures. Casey *et al.* [2006] reported that the  $\sim N$  trending faults ( $N10^{\circ} E$ ) displace historical fissure lava flows erupted from the southern flank of the Fantale volcano in 1810 and 1820 [e.g., Williams *et al.*, 2004]. Hunt *et al.* [2019] suggest that the rectilinear, northern caldera margin may be controlled by a fault (Figure 2b). Finally, Temtime *et al.* [2020] investigated and modelled rhyolitic dyke intrusion accompanied by ground fractures that occurred in 2015 NW of Fantale Caldera. The trend of the ground fractures ranges

between  $\sim 35^{\circ}$  and  $5^{\circ}$  and the modelling suggested that the dyke strike  $\sim 29^{\circ} \pm 2^{\circ}$  [Temtime *et al.*, 2020].

### 3.1.3. Kone volcanic complex (KVC)

The Kone volcanic complex (KVC, Rampey *et al.*, 2010; Figures 1 and 2c; Table 1), also referred as Gariboldi, is a major Quaternary composite caldera system where at least seven Pleistocene to Recent caldera collapses (with eruption in historic period) were recognised [Mohr, 1962a, Cole, 1969, Rampey *et al.*, 2010]. Located  $\sim 30$  km SW of Fantale, it represents the northern tip of the so-called Boset–Kone Magmatic segment (Figure 1) and is composed of three superimposed major caldera depressions, respectively named Birenti, which is nowadays visible as several isolated segments of caldera wall, Kone and Korke [Cole, 1969, Rampey *et al.*, 2010]. The nature of the remnants of the caldera walls suggest that the Birenti Caldera is composed of at least two nested calderas (Figure 2c), with an inferred diameter of  $\sim 11$  km and an area of  $\sim 95$  km<sup>2</sup> for this composite caldera collapse that is the oldest of the KVC [Rampey *et al.*, 2010]. Other data about the KVC can be found in Table 1.

The Kone Caldera rim is described by Rampey *et al.* [2010] as a horseshoe structure opening to E with the northern portion of the rim extending SW ( $\sim 350$  m), where  $\sim 200$  m of caldera wall material are exposed together with  $\sim 150$  m of pyroclastic caldera forming deposits (Figure 2c). Rampey *et al.* [2010] reported that the Kone Caldera wall is moderately incised by post collapse erosion and that the southern part of the western margin is cut by a E–W trending fault. In the surrounding areas, Acocella *et al.* [2002] mapped NNE–SSW trending WFB faults ( $N20^{\circ} \pm 3^{\circ}$ ) (Figure 5), and described alignments of monogenic vents in the eastern portion of the caldera, trending approximately  $N17^{\circ}$ , therefore subparallel to regional NNE–SSW faults.

### 3.1.4. Gedemsa caldera

The Gedemsa Caldera is located east of Lake Koka,  $\sim 80$  km south of the KVC (Figure 1), along the axial part of the MER [Acocella *et al.*, 2002] and in the proximity of the northern tip of the Aluto–Gedemsa magmatic segment [Casey *et al.*, 2006 and reference therein; Figure 1]. Its activity, clustered in three distinguishable phases (pre-caldera, caldera and post caldera activity), as detailed by Hutchison *et al.*

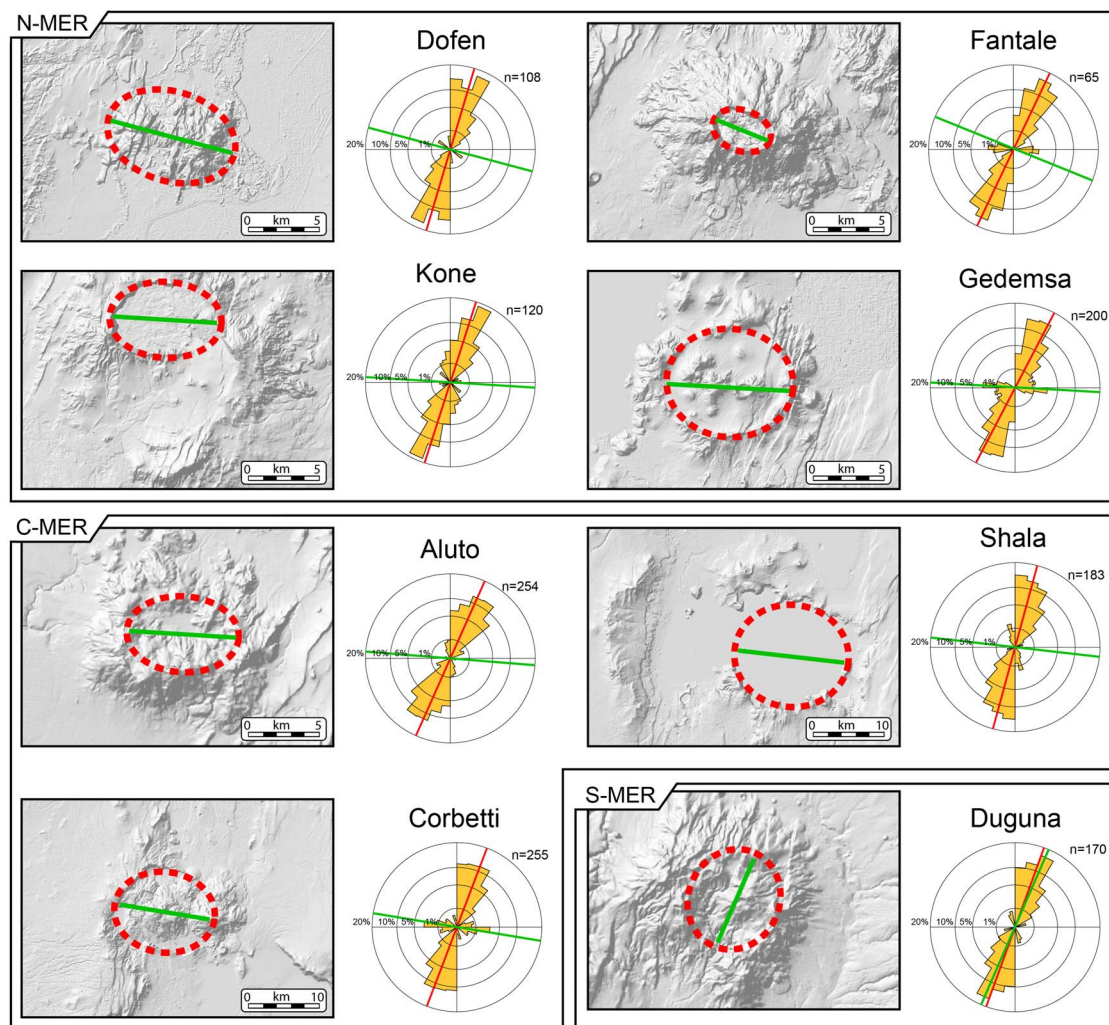


**Figure 5.** Caldera elongation and regional structures orientation for the examined volcanic and caldera complexes in along the MER. Rose diagram (length weighted) shows mapped tectonic structures reported in Figures 2, 3 and 4. Red line indicate the average trend of tectonic structures while green lined shows the trend of caldera elongation corresponding to the caldera major axis (see also Table 1). Red thick dashed lines indicate the inferred geometry of the calderas.

[2016a] and Hunt *et al.* [2019], mainly produced silicic with few subordinated mafic and intermediate products [e.g., Di Paola, 1972]. Lavas (trachytes, rhyolites and obsidians) and pyroclastics (ignimbrites, surges and fallout) were mainly erupted, compositionally ranging from hawaiite to rhyolite, with mafic components erupted only during post-caldera activity [Peccherillo *et al.*, 1995]. Di Paola [1972] indicated that the NNE–SSW regional faults affect the col-

lapsed caldera, especially in its eastern portion. Hunt *et al.* [2019] suggest that some of the caldera margins, expressed as rectilinear faults may be controlled by inherited structures (Figure 2d). Acocella *et al.* [2002] identified the same NNE–SSW trending faults and characterized them as extensional WFB fractures and faults (average trend  $N22^\circ \pm 3^\circ$ ) with maximum vertical displacement of  $\sim 100$  m (Figures 2d and 5; Table 1). The northern and southern rims have an

E–W strike, while to the west and to the east NNE–SSW rectilinear faults mark the caldera rim, defining an overall rhomboidal shape.

### 3.2. C-MER calderas

#### 3.2.1. Aluto caldera

Aluto is a major silicic eruptive centre situated in the tectonically controlled lacustrine Ziway-Shala basin [e.g., Di Paola, 1972, Le Turdu *et al.*, 1999, Benvenuti *et al.*, 2002], which experienced caldera collapse with large explosions and associated extensive ignimbrite deposits [Hutchison *et al.*, 2015, 2016b]. This volcano lays between the Gademotta Caldera remnants (20 km to the NE) and the Munesa Caldera remnants to the South, the latter being masked by Lake Langanu (Figure 3). These two large silicic calderas, nowadays exposed only in scattered and highly eroded portions, ceased their activity before 1 Ma and are considered two of the largest calderas developed along the MER [Hutchison *et al.*, 2016b, and reference therein; Table 1]. A detailed description of the Aluto eruptive history is provided by Hutchison *et al.* [2016a,b], which defined a three-stage evolution, depicting pre-caldera, caldera and post-caldera activity. Nowadays, the Aluto Caldera shows a marked E–W trending elongation (Figure 5), despite no major faults with a similar trend are observed inside the depression, or outside, in the proximity of the caldera (Figure 3a). At places, the caldera rims are dissected by N–NE-trending Wonji faults (Figure 5), which are absent in the area between Aluto and Gademotta remnants. Higher density of such faults is observed east of the Aluto Caldera, near the remnants of the Munesa Caldera, where several faults structures are visible in correspondence of the Lake Langanu banks (Figure 3a) and that extends also below the lake surface, as highlighted by geophysical data [Le Turdu *et al.*, 1999].

#### 3.2.2. Shala (O'a) caldera

Shala, or O'a, Caldera lays  $\approx 40$  km south of the Aluto Caldera, in an area that is completely obscured by Lake Shala. The most evident remnants of this large collapse (that occurred around 0.24 Ma, Mohr *et al.*, 1980, Le Turdu *et al.*, 1999, Table 1) are the northern and southern scarps, which mostly cut ignimbrites and pumices and subordinately rhyolitic lavas [Di Paola, 1972]. Toward east and west, the

caldera margins were eroded and the entire caldera edifice including the caldera ring faults were masked by the lake [Mohr *et al.*, 1980]. Connection of rim remnants suggests a limited E–W elongation of the caldera collapse area (Figure 5, Table 1), but no direct data can be obtained about internal caldera structure and morphology. Several faults belonging to the WFB are visible around the Lake Shala with an overall NNE–SSW trend, some of which were named by Le Turdu *et al.* [1999] as Southern Shala Fault System and Eastern Shala Fault System (Figure 3b). The WFB was active during the Shala volcanic complex evolution and appears to have been active up to the Holocene [Mohr *et al.*, 1980, Le Turdu *et al.*, 1999]. No E–W trending faults are observed in the caldera proximity (Figure 3b), but Mohr *et al.* [1980] report sparse ESE-trending transverse faults on the caldera eastern side.

#### 3.2.3. Corbetti caldera and Awasa caldera remnants

The Corbetti Caldera is located  $\approx 30$  km southwest of the Shala Caldera, close to the Awasa (or Hawassa) Caldera remnants in the Lake Awasa Basin [Hutchison *et al.*, 2016a; Figure 3c]. The Corbetti Caldera has been the object of many studies in the past and in recent times, which have detailed its major features [Di Paola, 1971, 1972, Hunt *et al.*, 2019; Table 1]. Besides, pre-caldera activity was followed at Corbetti by large ignimbrite eruption and caldera formation around  $182 \pm 28$  ka BP [Hutchison *et al.*, 2016a]. Based on geodetic and magnetotelluric data, Lloyd *et al.* [2018] hypothesize the presence of a  $\approx$ E–W trending regional structures extending down to  $\sim 30$  km in the crust and associated magma emplacement and caldera collapse elongation (Figure 5). Intra-caldera structures show a similar trend (Figures 3a and 5) and crosscut the inferred caldera rim on its eastern side, and align with post-caldera volcanic emission points. Nonetheless, outside the caldera no E–W trending structures are observed, and faults in the Corbetti–Awasa area show an NNE–SSW trend consistent with the WFB (Figure 5). Hunt *et al.* [2019] report that some of the caldera margins characterised by a rectilinear trend may be controlled by faults (Figure 3c). The Awasa remnants, covering an area of  $\approx 35 \times 20$  km (Table 1), testify a much larger collapse (one of the three largest occurred along the C-MER, with Munesa and Gademotta collapses; Hutchison *et al.*, 2016b, and references therein). This

caldera experienced its major caldera-forming eruption around 1.85–1.1 Ma [WoldeGabriel *et al.*, 1990] and is nowadays strongly eroded, with the caldera floor partly obscured by Lake Awasa.

### 3.3. S-MER calderas

#### 3.3.1. Duguna and Hobitcha

The Duguna Caldera [Newhall and Dzurisin, 1988] is a large volcanic centre located at the northernmost tip of the S-MER,  $\approx 20$  km southwest of the Awasa Caldera. This volcanic complex shows a summit caldera collapse, which produced pumices and ashfall deposits [Chernet, 2011], roughly elongated along a NE–SW trend (Figures 4 and 5), and covers an approximate area of  $\approx 8 \times 6$  km (Table 1). Ages of 430–460 ka have been reported for the eastern flank of the Duguna volcano [Bigazzi *et al.*, 1993; Table 1]. The pre-caldera volcanic edifice is crosscut by NE–SW trending rift boundary faults (Figures 4 and 5), and Wonji faults with a similar trend surface southeast of Duguna, along the axial sector of the MER [Corti *et al.*, 2013]. The boundary faults also seem to align with several minor volcanic emission points and crosscut the remnant of the larger Hobitcha Caldera remnants, a horseshoe-shaped rhyolitic centre, with a diameter of  $\sim 10$  km [Chernet, 2011, Corti *et al.*, 2013; Table 1].

## 4. Discussion: interaction between calderas and regional tectonics in the MER

The direction of extension along the MER was reconstructed by several authors based on structural data and GPS vectors, suggesting a direction of horizontal stretching ranging between N135° E and N105° E [e.g., Chorowicz *et al.*, 1994, Bilham *et al.*, 1999, Chu and Gordon, 1999, Acocella *et al.*, 2002, Keir *et al.*, 2006]. Nonetheless, other studies suggested a partly different extension direction trending around N90°–100° [e.g., Bonini *et al.*, 1997, Boccaletti *et al.*, 1998, Fernandes *et al.*, 2004, Pizzi *et al.*, 2006, Agostini *et al.*, 2011b, Saria *et al.*, 2014, Stamps *et al.*, 2021]. It is well known that elongated calderas may reflect the regional stress field [e.g., Bosworth *et al.*, 2000, 2003] and thus extension along the MER may have controlled caldera elongation [Casey *et al.*, 2006]. Notably, the elongation of the examined calderas

(except for the summit Duguna Caldera) is mostly parallel to the proposed N90°–100° trending extension direction acting on the MER (Figure 5).

Nonetheless, several mechanisms were proposed in literature to justify caldera elongation and the trend of associated volcano-tectonic features (e.g., vent alignments). Robertson *et al.* [2015] summarized the main mechanism to explain caldera elongation along the Kenya Rift. These authors report that caldera elongated shape may be induced by (i) the pre-collapse elongation of the underlying magma chamber (Figure 6a, b, c), which may be in turn driven by other processes, as explained below, (ii) poly-phased collapse resulting into nested calderas (Figure 6d), assuming an overall elongated geometry, (iii) fault-controlled caldera rim (Figure 6e) and (iv) post-collapse events or continued stretching (Figure 6f, g). More specifically, the elongation of the magma chamber can depend upon magma migration and emplacement along pre-existing structures [e.g., Montanari *et al.*, 2020; Figure 6c] or by the orientation of the stress field (Figure 6a, b), such that the long caldera axis may be parallel to the minimum horizontal stress (Figure 6a), assuming a mechanism analogue to borehole breakout [e.g., Bosworth *et al.*, 2000, 2003], or the maximum horizontal stress [Figure 6b; e.g., Wadge *et al.*, 2016]. In this frame, the analysis of associated volcanic features may help to discern between the two latter cases [e.g., Bonini, 2012]. Poly-phased collapse is likely the simplest mechanism to explain caldera elongation: subsequent collapse and nested caldera formation may in fact induce an apparent composite caldera elongation, which may, or may not, reflect an underlying elongated magma chamber (Figure 6d). Collapse may induce caldera elongation when in presence of inherited linear crustal structures, reactivated during the collapse or when distorted by local structures [e.g., Acocella *et al.*, 2002, 2004, Holohan *et al.*, 2005, 2008, Maestrelli *et al.*, 2020, 2021a,b] (i.e., fault-controlled caldera rim, Figure 6e). Post-collapse events can finally at least in part contribute to create elongated caldera depressions (e.g., post collapse erosion or continued strain due to regional stretching after caldera collapse, Figure 6f, g). These mechanisms, summarized by Robertson *et al.* [2015], can be considered valid worldwide and therefore, their applicability can be also tested for calderas occurring along the MER.

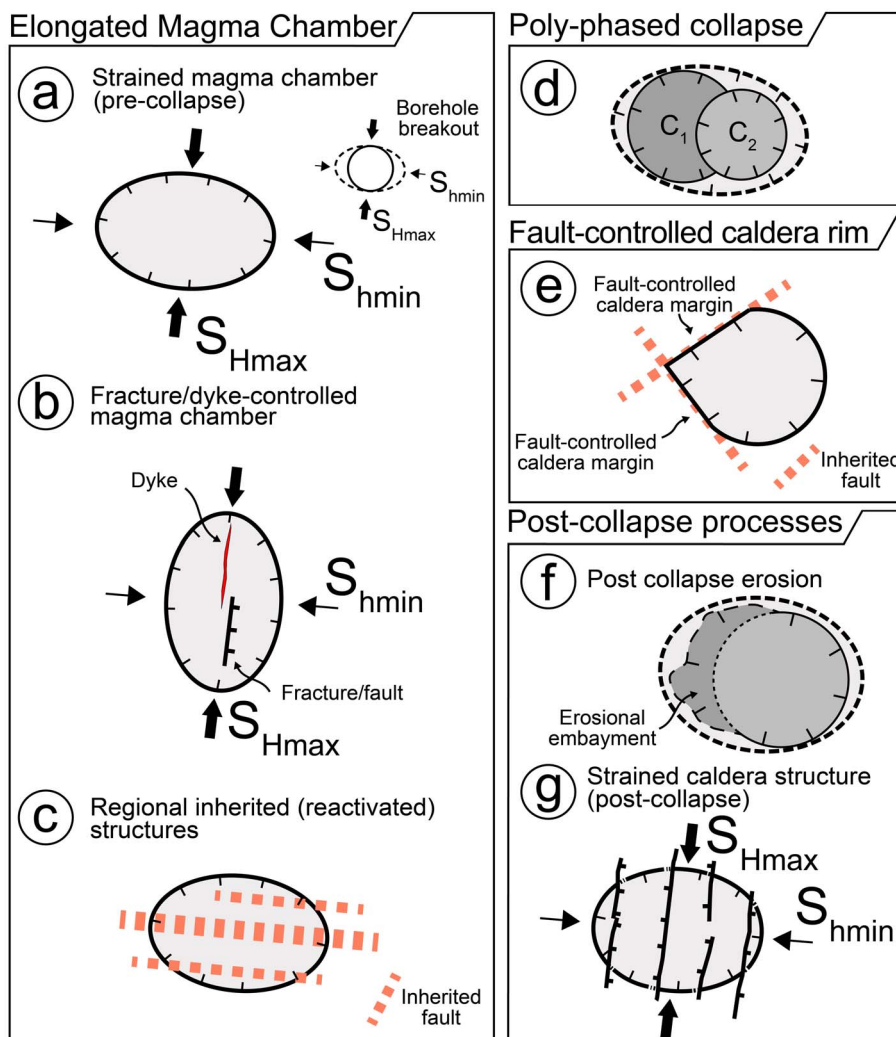


**Figure 6.** Sketch inspired and modified from Robertson *et al.* [2015, and reference therein] summarizing the possible mechanisms contributing to caldera elongation. (a–c) Caldera elongation controlled by an elongated magma chamber. This may occur as a result of (a) tectonic strain (in analogy to the borehole breakout mechanism; e.g., Mazzarini *et al.*, 2010), (b) elongation along induced fractures/dykes or (c) magma emplacement along regional reactivated structures. (d) Nested collapse may control the overall composite caldera elongation. (e) The presence of existing discontinuities can produce elongated caldera depressions. Other shallow crustal processes (not shown in the figure; e.g., asymmetrical subsidence, pre-collapse topography) can produce similar elongation [Robertson *et al.*, 2015]. (f–g) Post-collapse processes, such as erosion or strain of the caldera structure due to regional stretching (i.e., parallel to the direction of extension and orthogonal to regional faults that therefore dissect the caldera structure), may finally contribute to the caldera elongation. See the text for details.  $S_{Hmax}$ : maximum horizontal stress;  $S_{hmin}$ : minimum horizontal stress;  $C_1$  and  $C_2$ : primary and subsequent collapses.

In this regard, Acocella *et al.* [2002] suggested a forcing of structural inheritance in controlling the elongation of the Fantale, Kone and Gedemsa calderas (Figures 2, 5). Nevertheless, no major ESE–WNW inherited structures (i.e., parallel to caldera elongation) are exposed in the surrounding areas of the caldera (Figures 2, 5), but they occur on the plateaus as large-throw sub-vertical faults, suggesting that they may be present as buried structures beneath the rift floor (Figure 6c). These sub-vertical regional structures may have been reactivated as left-lateral strike slip structures during E–W rifting, creating preferential local areas of unclamping favourable for magma ascent and emplacement, consequently forcing caldera elongation and generating vent alignments (Figure 6c). In this model, the Wonji faults do not control the caldera structural setting and simply influence post-caldera activity by localizing points of emission outside the caldera [Acocella *et al.*, 2002, Fontijn *et al.*, 2018]. At the Corbetti Caldera (Figures 3, 5), Lloyd *et al.* [2018] hypothesize the presence of an E–W trending regional structure extending downward into the crust for at least 30 km. They propose that these structures may be related to the Goba-Bonga lineament, as also supported by detailed geological-structural analysis [Corti *et al.*, 2018] and geophysical data [Lavayssière *et al.*, 2019], and suggest a similar model to Acocella *et al.* [2002] for magma emplacement and caldera elongation. Conversely, Casey *et al.* [2006] suggested an active role of regional stretching on the elongation of the calderas along the MER, as the mechanism sketched in Figure 6g. Besides, the regional stress field may induce magma chamber elongation, as sketched in Figure 6a. In our interpretation, these two mechanism can explain the average E–W to ESE–WNW trend of caldera elongation along the MER, which is coherent with the  $\approx$ E–W direction of regional extension (cf. with Figure 5). Out of the examined calderas, only Duguna shows a moderate NNE–SSW elongation (Figure 5), and we speculate that it may follow the trend of regional structures (Figure 6b), which is there represented by the boundary faults (Figure 4).

Poly-phased collapse, producing nested calderas, was suggested by Rampey *et al.* [2010] for the Kone Caldera, in contrast with the hypothesis of a tectonic control exerted by E–W regional structures proposed by Acocella *et al.* [2002], as well as with the stretching of the magma chamber under regional

stress. Likely, poly-phased collapse also occurred at other calderas along the MER (e.g., Shala Caldera). Nonetheless, for several calderas showing marked elongation, it unlikely represents the main mechanism leading to an elliptical shape, since no other major nested calderas are observed (e.g. Fantale, Aluto and Corbetti calderas).

Inherited local structures may have played a role during the collapse of specific calderas along the MER (e.g., reactivated as caldera faults). For example, some margins of the Fantale, Kone, Gedemsa and Corbetti calderas (Figures 2 and 3) are indicated by Acocella *et al.* [2002] and Hunt *et al.* [2019] as fault-controlled, and likely resulted from the reactivation of inherited structures during the collapse (Figure 6e).

Although post-caldera erosion (Figure 6f) represents an active mechanism occurring at several calderas, as testified by many embayments visible along caldera margins [Hunt *et al.*, 2019; e.g., Awasa and Shala calderas, Figure 3b, c], this process seems to act at a different (smaller) scale to justify the marked elongation of some of the examined calderas (e.g., Fantale, Corbetti), where caldera margins are still well traceable. Therefore, in our interpretation it cannot be considered as a main mechanism shaping elongated calderas in the MER.

Overall, based on the above considerations, we infer that elongation of the magmatic chamber and the regional stretching are the most effective mechanism controlling the elliptical caldera geometry of the considered MER calderas (Figure 5). As noted earlier, the first process may reflect the influence of the regional stress (Figure 6a) or possibly the effect exerted by inherited crustal structures along which magma is preferentially emplaced as an oblate magma body, resulting afterward in an elongated collapse (Figure 6c). Beside, regional stretching may at least in part contribute to elongate calderas after collapse [Casey *et al.*, 2006; Figure 6g], as several calderas are dissected by regional faults trending to an high angle to the caldera major axis (i.e., the caldera elongation; Figure 5). Nonetheless, this mechanism cannot represent the exclusive mechanism, as normal faults observed in the area are not sufficient to justify caldera elongation. We therefore suggest that these processes (i.e., magmatic chamber elongation, inherited crustal structures reactivation and regional stretching) are the main concurring mechanisms driving the forma-

tion of elongated calderas along the MER, although other processes may contribute to caldera elongation globally (Figure 6d, e, f).

## 5. Concluding remarks

In this study, we have reviewed the structural characteristics of the main collapsed calderas that occur along the axis of the Northern, Central and Southern sectors of the Main Ethiopian Rift. These peralkaline calderas bear a strong linkage with the tectonics of this continental rift, showing several features suggesting a tectonic control on their development. Specifically, most of the examined calderas have a moderate to marked elongation and some of them (e.g., Fantale, Kone, Gedemsa and Corbetti calderas) have experienced a tectonic control exerted by pre-existing faults reactivated during the collapse (i.e., fault-controlled caldera rim; Figure 6e). Although poly-phased collapse leading to nested calderas (Figure 6d) may explain the elongation of some of the examined calderas (e.g., Shala and Kone volcanic complexes), it is not observed at other calderas, for which different mechanisms should be taken into account. Finally, post-collapse processes (e.g., caldera erosion; Figure 6f) likely act at a different (local) scale to justify markedly elongated calderas. We therefore propose that the main mechanisms responsible for caldera elongation along the MER are likely related to the elongation of the subsurface magma body and to regional stretching. Magma chamber elongation may depend on the regional stress field (Figure 6a, b) or the presence of regional existing structures reactivated during the emplacement of magma (Figure 6c). Regional stretching may at least partly contribute to elongate circular collapsed calderas (Figure 6g). Nonetheless, future studies are required to better define the main controls on caldera development and elongation in the MER, as well as to further investigate the relationships with tectonic processes.

## Acknowledgements

We would like to thank Bruno Scaillet for inviting us to contribute to this special Volume. We are grateful to Hugues Raimbourg and to an anonymous Reviewer for their helpful comments that greatly improved the quality of our manuscript. This work has been funded by the Italian Ministero

dell'Università e della Ricerca (MiUR) through PRIN Grant 2017P9AT72.

## References

- Acocella, V. (2007). Understanding caldera structure and development: An overview of analogue models compared to natural calderas. *Earth Sci. Rev.*, 85(3–4), 125–160.
- Acocella, V., Funicello, R., Marotta, E., Orsi, G., and De Vita, S. (2004). The role of extensional structures on experimental calderas and resurgence. *J. Volcanol. Geotherm. Res.*, 129(1–3), 199–217.
- Acocella, V., Korme, T., Salvini, F., and Funicello, R. (2002). Elliptic calderas in the Ethiopian Rift: control of pre-existing structures. *J. Volcanol. Geotherm. Res.*, 119(1–4), 189–203.
- Agostini, A., Bonini, M., Corti, G., Sani, F., and Manetti, P. (2011b). Distribution of Quaternary deformation in the central main Ethiopian rift, East Africa. *Tectonics*, 30, article no. TC4010.
- Agostini, A., Bonini, M., Corti, G., Sani, F., and Mazzarini, F. (2011a). Fault architecture in the Main Ethiopian Rift and comparison with experimental models: implications for rift evolution and Nubia–Somalia kinematics. *Earth Planet. Sci. Lett.*, 301(3–4), 479–492.
- Balestrieri, M. L., Bonini, M., Corti, G., Sani, F., and Philippson, M. (2016). A refinement of the chronology of rift-related faulting in the Broadly Rifted Zone, southern Ethiopia, through apatite fission-track analysis. *Tectonophysics*, 671, 42–55.
- Bastow, I. D., Nyblade, A. A., Stuart, G. W., Rooney, T. O., and Benoit, M. H. (2008). Upper mantle seismic structure beneath the Ethiopian hot spot: rifting at the edge of the African low-velocity anomaly. *Geochemistry, Geophys. Geosystems*, 9, article no. Q12022.
- Bastow, I. D., Pilidou, S., Kendall, J. M., and Stuart, G. W. (2010). Melt-induced seismic anisotropy and magma assisted rifting in Ethiopia: evidence from surface waves. *Geochemistry, Geophys. Geosystems*, 11(6). <https://doi.org/10.1029/2010GC003036>.
- Bastow, I. D., Stuart, G. W., Kendall, J. M., and Ebinger, C. J. (2005). Upper-mantle seismic structure in a region of incipient continental breakup: northern Ethiopian rift. *Geophys. J. Int.*, 162(2), 479–493.
- Benvenuti, M., Carnicelli, S., Belluomini, G., Dainelli, N., Di Grazia, S., Ferrari, G. A., Iasio, C., Sagri,

- M., Ventra, D., Atnafu, B., and Kebede, S. (2002). The Ziway–Shala lake basin (main Ethiopian rift, Ethiopia): a revision of basin evolution with special reference to the Late Quaternary. *J. Afr. Earth Sci.*, 35(2), 247–269.
- Bigazzi, G., Bonadonna, F. P., Di Paola, G. M., and Giuliani, A. (1993). K–Ar and fission track ages of the last volcano-tectonic phase in the Ethiopian Rift Valley (Tullu Moye area). In Abbate, E., Sagri, M., and Sassi, F. P., editors, *Geology and Mineral Resources of Somalia and Surrounding Regions*, volume 113 of *Relazi Monogr. Agrarie Subtrop. Trop.*, pages 311–322. Ist. Agron. per l’Oltremare, Florence, Italy.
- Bilham, R., Bendick, R., Larson, K., Mohr, P., Braun, J., Tesfaye, S., and Asfaw, L. (1999). Secular and tidal strain across the Main Ethiopian Rift. *Geophys. Res. Lett.*, 26(18), 2789–2792.
- Boccaletti, M., Bonini, M., Mazzuoli, R., Abebe, B., Piccardi, L., and Tortorici, L. (1998). Quaternary oblique extensional tectonics in the Ethiopian Rift (Horn of Africa). *Tectonophysics*, 287(1–4), 97–116.
- Boccaletti, M., Mazzuoli, R., Bonini, M., Trua, T., and Abebe, B. (1999). Plio-Quaternary volcanotectonic activity in the northern sector of the Main Ethiopian Rift: relationships with oblique rifting. *J. Afr. Earth Sci.*, 29(4), 679–698.
- Bonini, M. (2012). Mud volcanoes: indicators of stress orientation and tectonic controls. *Earth Sci. Rev.*, 115(3), 121–152.
- Bonini, M., Corti, G., Innocenti, F., Manetti, P., Mazzarini, F., Abebe, T., and Pecskey, Z. (2005). Evolution of the Main Ethiopian Rift in the frame of Afar and Kenya rifts propagation. *Tectonics*, 24(1), article no. TC1007.
- Bonini, M., Maestrelli, D., Corti, G., Del Ventisette, C., Moratti, G., Carrasco-Núñez, G., Giordano, G., Lucci, F., Norini, G., Piccardi, L., Urbani, S., and Montanari, D. (2021). Modeling intra-caldera resurgence settings: laboratory experiments with application to the Los Humeros Volcanic Complex (Mexico). *J. Geophys. Res. Solid Earth*, 126(3), article no. e2020JB020438.
- Bonini, M., Sokoutis, D., Mulugeta, G., Boccaletti, M., Corti, G., Innocenti, F., Manetti, P., and Mazzarini, F. (2001). Dynamics of magma emplacement in centrifuge models of continental extension with implications for flank volcanism. *Tectonics*, 20, 1053–1065.
- Bonini, M., Souriot, T., Boccaletti, M., and Brun, J. P. (1997). Successive orthogonal and oblique extension episodes in a rift zone: laboratory experiments with application to the Ethiopian Rift. *Tectonics*, 16(2), 347–362.
- Bosworth, W., Burke, K., and Strecker, M. (2000). Magma chamber elongation as an indicator of intraplate stress field orientation: “borehole breakout mechanism” and examples from the Late Pleistocene to Recent Kenya Rift Valley. In: (Ed.) Mark Jessell, and Janos Urai, Stress strain and structure, a volume in honour of Win D. Means. *J. Virtual Explor.*, 2, article no. 5. Electronic Edition, ISSN 1441-8142.
- Bosworth, W., Burke, K., and Strecker, M. (2003). Effect of stress fields on magma chamber stability and the formation of collapse calderas. *Tectonics*, 22(4). <https://doi.org/10.1029/2002TC001369>.
- Casey, M., Ebinger, C., Keir, D., Gloaguen, R., and Mohamed, F. (2006). Strain accommodation in transitional rifts: extension by magma intrusion and faulting in Ethiopian rift magmatic segments. *Geol. Soc. Lond. Spec. Publ.*, 259(1), 143–163.
- Chernet, T. (2005). Geological and hydrothermal alteration mapping of the Dofen geothermal prospect and adjacent western escarpment (Ethiopia). In *Proceedings of the World Geothermal Congress, Antalya, Turkey*, pages 24–29.
- Chernet, T. (2011). Geology and hydrothermal resources in the northern Lake Abaya area (Ethiopia). *J. Afr. Earth Sci.*, 61(2), 129–141.
- Chernet, T. and Hart, W. K. (1999). Petrology and geochemistry of volcanism in the northern Main Ethiopian Rift-southern Afar transition region. *Acta Vulcanol.*, 11, 21–42.
- Chorowicz, J., Collet, B., Bonavia, F. F., and Korme, T. (1994). Northwest to north-northwest extension direction in the Ethiopian rift deduced from the orientation of extension structures and fault-slip analysis. *Geol. Soc. Am. Bull.*, 106(12), 1560–1570.
- Chu, D. and Gordon, R. G. (1999). Evidence for motion between Nubia and Somalia along the Southwest Indian Ridge. *Nature*, 398(6722), 64–67.
- Cole, J. W. (1969). Gariboldi volcanic complex, Ethiopia. *Bull. Volcanol.*, 33(2), 566–578.
- Corti, G. (2008). Control of rift obliquity on the evolution and segmentation of the main Ethiopian rift. *Nat. Geosci.*, 1, 258–262.
- Corti, G. (2009). Continental rift evolution: from



- rift initiation to incipient break-up in the Main Ethiopian Rift, East Africa. *Earth Sci. Rev.*, 96(1–2), 1–53.
- Corti, G., Cioni, R., Franceschini, Z., Sani, F., Scaillet, S., Molin, P., Isola, I., Mazzarini, F., Brune, S., Keir, D., Erbello, A., Muluneh, A., Illsley-Kemp, F., and Glerum, A. (2019). Aborted propagation of the Ethiopian rift caused by linkage with the Kenyan rift. *Nat. Commun.*, 10(1), 1–11.
- Corti, G., Sani, F., Agostini, S., Philippon, M., Sokoutis, D., and Willingshofer, E. (2018). Off-axis volcano-tectonic activity during continental rifting: Insights from the transversal Goba-Bonga lineament, Main Ethiopian Rift (East Africa). *Tectonophysics*, 728, 75–91.
- Corti, G., Sani, F., Philippon, M., Sokoutis, D., Willingshofer, E., and Molin, P. (2013). Quaternary volcano-tectonic activity in the Soddo region, western margin of the Southern Main Ethiopian Rift. *Tectonics*, 32(4), 861–879.
- Di Paola, G. M. (1971). Geology of the Corbetti Caldera area (Main Ethiopian Rift Valley). *Bull. Volcanol.*, 35(2), 497–506.
- Di Paola, G. M. (1972). The Ethiopian Rift Valley (between 7°00' and 8°40' lat. north). *Bull. Volcanol.*, 36(4), 517–560.
- Druitt, T. H. and Sparks, R. S. J. (1984). On the formation of calderas during ignimbrite eruptions. *Nature*, 310(5979), 679–681.
- Ebinger, C. J. and Casey, M. (2001). Continental breakup in magmatic provinces: an Ethiopian example. *Geology*, 29(6), 527–530.
- Fernandes, R. M. S., Ambrosius, B. A. C., Noomen, R., Bastos, L., Combrinck, L., Miranda, J. M., and Spakman, W. (2004). Angular velocities of Nubia and Somalia from continuous GPS data: implications on present-day relative kinematics. *Earth Planet. Sci. Lett.*, 222(1), 197–208.
- Fontijn, K., McNamara, K., Tadesse, A. Z., Pyle, D. M., Dessalegn, E., Hutchison, W., Mather, T. A., and Yirgu, G. (2018). Contrasting styles of post-caldera volcanism along the Main Ethiopian Rift: implications for contemporary volcanic hazards. *J. Volcanol. Geotherm. Res.*, 356, 90–113.
- Geyer, A. and Marti, J. (2008). The new worldwide collapse caldera database (CCDB): a tool for studying and understanding caldera processes. *J. Volcanol. Geotherm. Res.*, 175(3), 334–354.
- Gibson, I. L. (1969). The structure and volcanic geology of an axial portion of the Main Ethiopian Rift. *Tectonophysics*, 8(4–6), 561–565.
- Giordano, F., D'Antonio, M., Civetta, L., Tonarini, S., Orsi, G., Ayalew, D., Yirgu, G., Dell'Erba, F., Di Vito, M. A., and Isaia, R. (2014). Genesis and evolution of mafic and felsic magmas at Quaternary volcanoes within the Main Ethiopian Rift: insights from Gedemsa and Fanta 'Ale complexes. *Lithos*, 188, 130–144.
- Gudmundsson, M. T., Jónsdóttir, K., Hooper, A., et al. (2016). Gradual caldera collapse at Bárðarbunga volcano, Iceland, regulated by lateral magma outflow. *Science*, 353(6296). <https://doi.org/10.1126/science.aaf8988>.
- Hayward, N. J. and Ebinger, C. J. (1996). Variations in the along-axis segmentation of the Afar Rift system. *Tectonics*, 15(2), 244–257.
- Holohan, E. P., de Vries, B. V. W., and Troll, V. R. (2008). Analogue models of caldera collapse in strike-slip tectonic regimes. *Bull. Volcanol.*, 70(7), 773–796.
- Holohan, E. P., Troll, V. R., Walter, T. R., Münn, S., McDonnell, S., and Shipton, Z. K. (2005). Elliptical calderas in active tectonic settings: an experimental approach. *J. Volcanol. Geotherm. Res.*, 144(1–4), 119–136.
- Hunt, J. A., Pyle, D. M., and Mather, T. A. (2019). The geomorphology, structure, and lava flow dynamics of peralkaline rift volcanoes from high-resolution digital elevation models. *Geochemistry, Geophys. Geosystems*, 20, 1508–1538.
- Hutchison, W., Fusillo, R., Pyle, D. M., Mather, T. A., Blundy, J. D., Biggs, J., Yirgu, G., Cohen, B. E., Brooker, R. A., Barfod, D. N., and Calvert, A. T. (2016a). A pulse of mid-Pleistocene rift volcanism in Ethiopia at the dawn of modern humans. *Nat. Commun.*, 7(1), 1–12.
- Hutchison, W., Mather, T. A., Pyle, D. M., Biggs, J., and Yirgu, G. (2015). Structural controls on fluid pathways in an active rift system: A case study of the Aluto volcanic complex. *Geosphere*, 11(3), 542–562.
- Hutchison, W., Pyle, D. M., Mather, T. A., Yirgu, G., Biggs, J., Cohen, B. E., Barfod, D. N., and Lewi, E. (2016b). The eruptive history and magmatic evolution of Aluto volcano: new insights into silicic peralkaline volcanism in the Ethiopian rift. *J. Volcanol. Geotherm. Res.*, 328, 9–33.
- Keir, D., Ebinger, C. J., Stuart, G. W., Daly, E., and

- Ayele, A. (2006). Strain accommodation by magmatism and faulting as rifting proceeds to breakup: seismicity of the northern Ethiopian rift. *J. Geophys. Res. Solid Earth*, 111(B5), article no. B05314.
- Kendall, J. M., Stuart, G. W., Ebinger, C. J., Bastow, I. D., and Keir, D. (2005). Magma-assisted rifting in Ethiopia. *Nature*, 433(7022), 146–148.
- Keranen, K. and Klemperer, S. L. (2008). Discontinuous and diachronous evolution of the Main Ethiopian Rift: implications for the development of continental rifts. *Earth Planet. Sci. Lett.*, 265, 96–111.
- Keranen, K., Klemperer, S. L., Gloaguen, R., and Group, E. W. (2004). Three-dimensional seismic imaging of a protoridge axis in the Main Ethiopian rift. *Geology*, 32(11), 949–952.
- Keranen, K., Klemperer, S. L., Julia, J., Lawrence, J. L., and Nyblade, A. (2009). Low lower-crustal velocity across Ethiopia: is the Main Ethiopian Rift a narrow rift in a hot craton? *Geochemistry, Geophys. Geosystems*, 10, article no. Q0AB01.
- Kieffer, B., Arndt, N., Lapiere, H., Bastien, F., Bosch, D., Pecher, A., Yirgu, G., Ayalew, D., Weis, D., Jerram, D. A., Keller, F., and Meugniot, C. (2004). Flood and shield basalts from Ethiopia: magmas from the African superswell. *J. Petrol.*, 45(4), 793–834.
- Korme, T., Chorowicz, J., Collet, B., and Bonavia, F. F. (1997). Volcanic vents rooted on extension fractures and their geodynamic implications in the Ethiopian Rift. *J. Volcanol. Geotherm. Res.*, 79(3–4), 205–222.
- Kurz, T., Gloaguen, R., Ebinger, C., Casey, M., and Abebe, B. (2007). Deformation distribution and type in the Main Ethiopian Rift (MER): a remote sensing study. *J. Afr. Earth Sci.*, 48(2–3), 100–114.
- Lavayssière, A., Greenfield, T., Keir, D., Ayele, A., and Kendall, J. M. (2019). Local seismicity near the actively deforming Corbetti volcano in the Main Ethiopian Rift. *J. Volcanol. Geotherm. Res.*, 381, 227–237.
- Le Turdu, C., Tiercelin, J.-J., Gibert, E., Travi, Y., Lezar, K.-E., Richert, J.-P., Massault, M., Gasse, F., Bonnefille, R., Decobert, M., Gensous, B., Jeudy, V., Tamrat, E., Mohammed, M. U., Martens, K., Atnafu, B., Chernet, T., Williamson, D., and Taieb, M. (1999). The Ziway–Shala lake basin system, Main Ethiopian Rift: influence of volcanism, tectonics, and climatic forcing on basin formation and sedimentation. *Palaeogeogr. Palaeoclimatol. Palaeoecol.*, 150(3–4), 135–177.
- Lipman, P. W. (1984). The roots of ash flow calderas in western North America: windows into the tops of granitic batholiths. *J. Geophys. Res. Solid Earth*, 89(B10), 8801–8841.
- Lipman, P. W. (1997). Subsidence of ash-flow calderas: relation to caldera size and magma-chamber geometry. *Bull. Volcanol.*, 59(3), 198–218.
- Lloyd, R., Biggs, J., Wilks, M., Nowacki, A., Kendall, J.-M., Ayele, A., Lewi, E., and Eysteinnsson, H. (2018). Evidence for cross rift structural controls on deformation and seismicity at a continental rift caldera. *Earth Planet. Sci. Lett.*, 487, 190–200.
- Maestrelli, D., Bonini, M., Corti, G., Del Ventisette, C., Moratti, G., and Montanari, D. (2021a). Exploring fault propagation and the role of inherited structures during caldera collapse through laboratory experiments. *J. Volcanol. Geotherm. Res.*, 414, article no. 107232.
- Maestrelli, D., Bonini, M., Corti, G., Del Ventisette, C., Moratti, G., and Montanari, D. (2021b). A database of laboratory analogue models of caldera collapse testing the role of inherited structures. *Front. Earth Sci.*, 9, article no. 618258.
- Maestrelli, D., Montanari, D., Corti, G., Del Ventisette, C., Moratti, G., and Bonini, M. (2020). Exploring the interactions between rift propagation and inherited crustal fabrics through experimental modeling. *Tectonics*, 39(12), article no. e2020TC006211.
- Mazzarini, F., Musumeci, G., Montanari, D., and Corti, G. (2010). Relations between deformation and upper crustal magma emplacement in laboratory physical models. *Tectonophysics*, 484, 139–146.
- Meyer, W., Pilger, A., Rosler, A., and Stets, J. (1975). Tectonic evolution of the northern part of the Main Ethiopian Rift in Southern Ethiopia. In Pilger, A. and Rosler, A., editors, *Afar Depression of Ethiopia*, pages 352–362. Schweizerbart, Stuttgart.
- Minissale, A., Corti, G., Tassi, F., Darrah, T. H., Vaselli, O., Montanari, D., Montegrossi, G., Yirgu, G., Selmo, E., and Teclu, A. (2017). Geothermal potential and origin of natural thermal fluids in the northern Lake Abaya area, Main Ethiopian Rift, East Africa. *J. Volcanol. Geotherm. Res.*, 336, 1–18.
- Mohr, P., Mitchell, J. G., and Reynolds, R. G. H. (1980). Quaternary volcanism and faulting at O'a Caldera, Central Ethiopian Rift. *Bull. Volcanol.*, 43(1), 173.
- Mohr, P. and Zanettin, B. (1988). The Ethiopian flood basalt province. In *Continental Flood Basalts*,

- pages 63–110. Springer, Dordrecht.
- Mohr, P. A. (1962a). Surface cauldron subsidence with associated faulting and fissure basalt eruptions at Gariboldi Pass, Shoa, Ethiopia. *Bull. Volcanol.*, 24(1), 421–428.
- Mohr, P. A. (1962b). The Ethiopian Rift system. *Bull. Geophys. Observ. Addis Ababa*, 5, 33–62.
- Mohr, P. A. (1967). The Ethiopian Rift system. *Bull. Geophys. Observ. Addis Ababa*, 11, 1–65.
- Mohr, P. A. and Wood, C. A. (1976). Volcano spacings and lithospheric attenuation in the Eastern Rift of Africa. *Earth Planet. Sci. Lett.*, 33(1), 126–144.
- Montanari, D., Del Ventisette, C., and Bonini, M. (2020). Lateral magma migration through interconnected sills: Evidence from analogue modeling. *Earth Planet. Sci. Lett.*, 551, article no. 116568.
- Morton, W. H., Rex, D. C., Mitchell, J. G., and Mohr, P. (1979). Riftward younging of volcanic units in the Addis Ababa region, Ethiopian rift valley. *Nature*, 280(5720), 284–288.
- Neal, C. A., Brantley, S. R., Antolik, L., et al. (2019). The 2018 rift eruption and summit collapse of Kīlauea Volcano. *Science*, 363(6425), 367–374.
- Newhall, C. G. and Dzurisin, D. (1988). *Historical Unrest at the Large Calderas of the World. Vol. 2*, volume 1855 of *US Geological Survey*. Department of the Interior.
- Peccerillo, A., Barberio, M. R., Yirgu, G., Ayalew, D., Barbieri, M., and Wu, T. W. (2003). Relationships between mafic and peralkaline silicic magmatism in continental rift settings: a petrological, geochemical and isotopic study of the Gedemsa volcano, central Ethiopian rift. *J. Petrol.*, 44(11), 2003–2032.
- Peccerillo, A., Gezahegn, Y., and Dereje, A. (1995). Genesis of acid volcanics along the Main Ethiopian Rift: a case history of the Gedemsa volcano. *Sinet*, 18(1), 23–50.
- Pizzi, A., Coltorti, M., Abebe, B., Disperati, L., Sacchi, G., and Salvini, R. (2006). The Wonji fault belt (Main Ethiopian Rift): structural and geomorphological constraints and GPS monitoring. *Geol. Soc. Lond. Spec. Publ.*, 259(1), 191–207.
- Rampey, M. L., Oppenheimer, C., Pyle, D. M., and Yirgu, G. (2010). Caldera-forming eruptions of the Quaternary Kone volcanic complex, Ethiopia. *J. Afr. Earth Sci.*, 58(1), 51–66.
- Robertson, E. A. M., Biggs, J., Cashman, K. V., Floyd, M. A., and Vye-Brown, C. (2015). Influence of regional tectonics and pre-existing structures on the formation of elliptical calderas in the Kenyan Rift. *Geol. Soc. Lond. Spec. Publ.*, 420(1), 43–67.
- Roche, O. and Druitt, T. H. (2001). Onset of caldera collapse during ignimbrite eruptions. *Earth Planet. Sci. Lett.*, 191(3–4), 191–202.
- Rooney, T. O. (2017). The Cenozoic magmatism of East-Africa: Part I—Flood basalts and pulsed magmatism. *Lithos*, 286, 264–301.
- Saria, E., Calais, E., Stamps, D. S., Delvaux, D., and Hartnady, C. J. H. (2014). Present-day kinematics of the East African Rift. *J. Geophys. Res. Solid Earth*, 119(4), 3584–3600.
- Sigmundsson, F. (2019). Calderas collapse as magma flows into rifts. *Science*, 366(6470), 1200–1201.
- Spera, F. J. and Crisp, J. A. (1981). Eruption volume, periodicity, and caldera area: relationships and inferences on development of compositional zonation in silicic magma chambers. *J. Volcanol. Geotherm. Res.*, 11(2–4), 169–187.
- Stamps, D. S., Kreemer, C., Fernandes, R., Rajaonarison, T. A., and Rambolamanana, G. (2021). Redefining East African Rift System kinematics. *Geology*, 49(2), 150–155.
- Temtime, T., Biggs, J., Lewi, E., and Ayele, A. (2020). Evidence for active rhyolitic dike intrusion in the Northern Main Ethiopian Rift from the 2015 Fentale Seismic Swarm. *Geochemistry, Geophys. Geosystems*, 21(6), article no. e2019GC008550.
- Trua, T., Deniel, C., and Mazzuoli, R. (1999). Crustal control in the genesis of Plio-Quaternary bimodal magmatism of the Main Ethiopian Rift (MER): geochemical and isotopic (Sr, Nd, Pb) evidence. *Chem. Geol.*, 155, 201–231.
- Wadge, G., Biggs, J., Lloyd, R., and Kendall, J. M. (2016). Historical volcanism and the state of stress in the East African Rift System. *Front. Earth Sci.*, 4, article no. 86.
- Williams, F. M., Williams, M. A. J., and Aumento, F. (2004). Tensional fissures and crustal extension rates in the northern part of the Main Ethiopian Rift. *J. Afr. Earth Sci.*, 38(2), 183–197.
- Williams, H. (1941). Calderas and their origin. *Univ. Calif. Publ. Geol. Sci.*, 21, 239–346.
- WoldeGabriel, G., Aronson, J. L., and Walter, R. C. (1990). Geology, geochronology, and rift basin development in the central sector of the Main Ethiopia Rift. *Geol. Soc. Am. Bull.*, 102, 439–458.
- WoldeGabriel, G., Walter, R. C., Aronson, J. L., and

Hart, W. K. (1992). Geochronology and distribution of silicic volcanic rocks of Plio-Pleistocene age from the central sector of the Main Ethiopian Rift. *Quat. Int.*, 13, 69–76.

WoldeGabriel, G., Walter, R. C., Hart, W. K., Mertzman, S. A., and Aronson, J. L. (1999). Temporal relations and geochemical features of felsic volcanism in the central sector of the Main Ethiopian Rift. *Acta Vulcanol.*, 11, 53–68.